SANDIA REPORT
SAND2009-2993
Unlimited Release
Printed May 2009

Radar Cross Section of Triangular Trihedral Reflector with Extended Bottom Plate

Armin W. Doerry and Billy C. Brock

Prepared by
Sandia National Laboratories
Albuquerque, New Mexico 87185 and Livermore, California 94550

Sandia is a multiprogram laboratory operated by Sandia Corporation,
a Lockheed Martin Company, for the United States Department of Energy's
National Nuclear Security Administration under Contract DE-AC04-94AL85000.

Approved for public release; further dissemination unlimited.

Sandia National Laboratories

Issued by Sandia National Laboratories, operated for the United States Department of Energy by Sandia Corporation.

NOTICE: This report was prepared as an account of work sponsored by an agency of the United States Government. Neither the United States Government, nor any agency thereof, nor any of their employees, nor any of their contractors, subcontractors, or their employees, make any warranty, express or implied, or assume any legal liability or responsibility for the accuracy, completeness, or usefulness of any information, apparatus, product, or process disclosed, or represent that its use would not infringe privately owned rights. Reference herein to any specific commercial product, process, or service by trade name, trademark, manufacturer, or otherwise, does not necessarily constitute or imply its endorsement, recommendation, or favoring by the United States Government, any agency thereof, or any of their contractors or subcontractors. The views and opinions expressed herein do not necessarily state or reflect those of the United States Government, any agency thereof, or any of their contractors.

Printed in the United States of America. This report has been reproduced directly from the best available copy.

Available to DOE and DOE contractors from
U.S. Department of Energy
Office of Scientific and Technical Information
P.O. Box 62
Oak Ridge, TN 37831

Telephone:		(865) 576-8401
Facsimile:		(865) 576-5728
E-Mail:		reports@adonis.osti.gov
Online	ordering:	http://www.osti.gov/bridge

Available to the public from
U.S. Department of Commerce
National Technical Information Service
5285 Port Royal Rd.
Springfield, VA 22161

Telephone:		(800) 553-6847
Facsimile:		(703) 605-6900
E-Mail:		orders@ntis.fedworld.gov
Online	order:	http://www.ntis.gov/help/ordermethods.asp?loc=7-4-0#online

SAND2009-2993
Unlimited Release
Printed May 2009

Radar Cross Section of Triangular Trihedral Reflector with Extended Bottom Plate

Armin Doerry
SAR Applications Department

Billy Brock
SAR Sensor Technologies Department

Sandia National Laboratories
PO Box 5800
Albuquerque, NM 87185-1330

Abstract

Trihedral corner reflectors are the preferred canonical target for SAR performance evaluation for many radar development programs. The conventional trihedrals have problems with substantially reduced Radar Cross Section (RCS) at low grazing angles, unless they are tilted forward, but in which case other problems arise. Consequently there is a need for better low grazing angle performance for trihedrals. This is facilitated by extending the bottom plate. A relevant analysis of RCS for an infinite ground plate is presented. Practical aspects are also discussed.

Approved for public release; further dissemination unlimited.

Acknowledgements

This report was funded by the Joint DoD/DOE Munitions Program Memorandum of Understanding project.

Contents

Foreword 6
1 Introduction 7
2 Radar Cross Section Calculation 9
2.1 Unit Triangular Trihedral with Infinite Ground Plate 9
2.2 Treating Bounces using Images 11
2.3 Calculating Projected Area 14
2.4 Calculating RCS 19
3 Comparison to Conventional Triangular Trihedral Corner Reflector 21
3.1 Review of Conventional Triangular Trihedral 21
3.2 Comparing Effects of Infinite Ground Plate 23
4 Some Practical Considerations 25
5 Validation 27
6 Conclusions 31
Appendix A – Rotated Coordinate Frame 33
Appendix B – Area of Triangle from Angle-Side-Angle Information 35
References 37
Distribution 38

Foreword

The genesis of this work was the need to develop better low grazing angle performance for canonical targets, those for which RCS can be relatively accurately calculated. Previous attempts to use conventional trihedrals tilted forward, sometimes on tripods, has offered ambiguous results, due to multipath phenomena. In addition, using conventional trihedrals with apex at ground level has led to RCS measurements exceeding the predicted free-space value, not surprisingly, due to ground-bounce. Consequently, the need became apparent to modify the conventional trihedral performance by altering its geometry to address these faults, and offer more predictable performance with greater RCS at low grazing angles.

1 Introduction

Trihedral corner reflectors are a canonical radar reflector frequently used to calibrate, or gauge the performance of radar systems. They offer the following desirable attributes.

- Fairly large Radar Cross Section (RCS) for its size.
- Fairly broad range of aspect angles with a large RCS.
- Theoretical RCS easily calculated as a function of aspect angle.

However, the following undesirable attributes also exist.

- The equations often provided for theoretical RCS assume the trihedral exists in free space, independent of surrounding environmental reflectors such as the ground.
- The RCS falls off rather dramatically as aspect angles approach parallel with the plates that make up the reflector.
- If a trihedral is tilted forward so that its direction of maximum RCS is at a shallow grazing angle with respect to the ground, then ground-lobing becomes problematic, diminishing the accuracy of the RCS calculations.
- If the trihedral is placed such that the bottom plate is parallel to the ground, then the RCS of the trihedral is severely diminished at low grazing angles with respect to the ground.

One solution is to build the trihedral corner reflector with an extended ground plate to enhance its RCS at low grazing angles without allowing ground-lobes to form.

In this report we examine the response of a triangular trihedral corner reflector composed of two upright isosceles right triangular plates on an infinitely large lower plate, as illustrated in Figure 1. More specifically, we will only really require an infinite quarter-plane, that is, infinite in extent in the quadrant of positive x and positive y values.

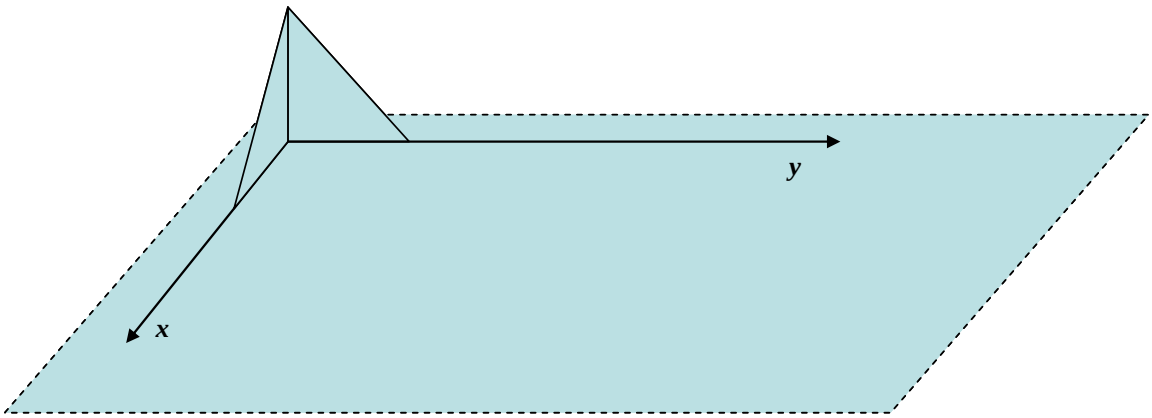

Figure 1. Triangular trihedral corner reflector on infinite conducting ground plane.

2 Radar Cross Section Calculation

To calculate the RCS of the triangular trihedral on infinite ground plane we will use a geometric optics model. This assumes that wavelength is small with respect to the dimensions of the trihedral.

We also note that RCS will then be proportional to the retro-reflecting area of the trihedral. Not all parts of the plates will contribute to a retro-reflection. The task at hand is to calculate the effective retro-reflecting area as a function of aspect angles. Once the area is calculated, then the RCS is given by

$$\sigma = \frac{4\pi}{\lambda^2} A^2 \quad (1)$$

where

λ = nominal wavelength of the radar, and
A = effective retro-reflecting area of the target. (2)

2.1 Unit Triangular Trihedral with Infinite Ground Plate

Consider a trihedral on an infinite ground plate with unit edges as illustrated in Figure 2.

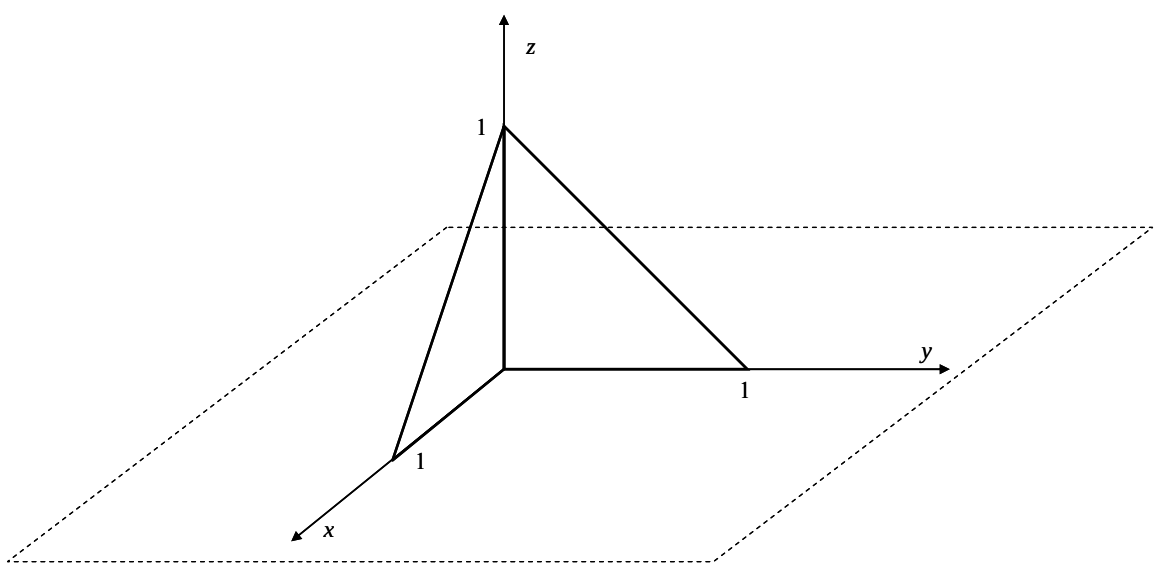

Figure 2. Unit dimension triangular trihedral on infinite ground plane.

Provided geometric optics still applies, the RCS will scale as the fourth power of the edge length. Now consider a viewing perspective defined by elevation and azimuth angles, as in Figure 3.

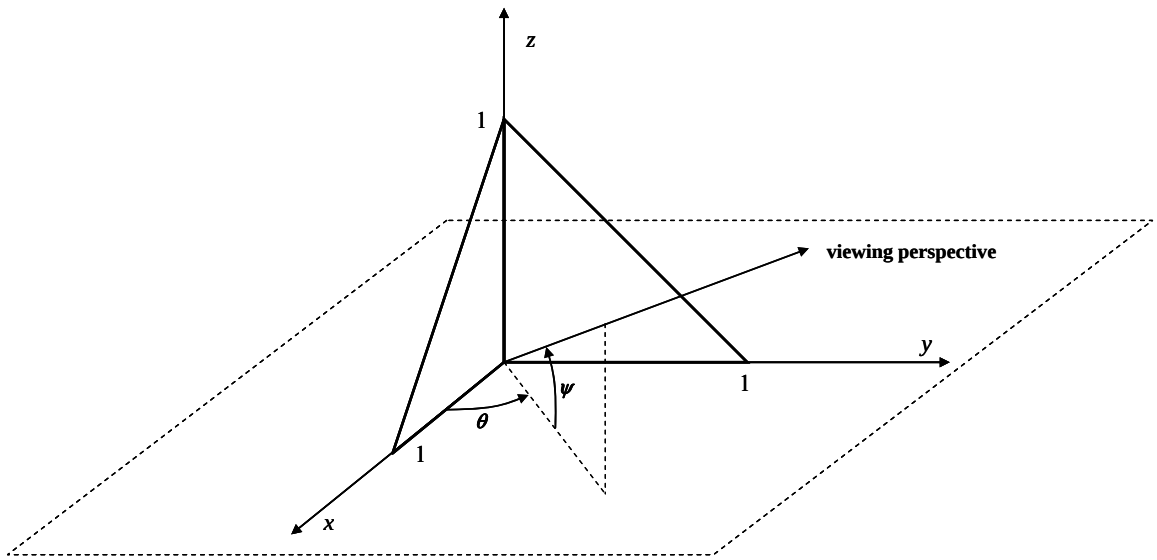

Figure 3. Definition of viewing perspective for trihedral corner reflector.

RCS will generally depend on the viewing perspective. We identify the viewing perspective with angles

θ = azimuth angle ($0 < \theta < \pi/2$), and
ψ = elevation angle ($0 < \psi < \pi/2$). (3)

The relevant points defining the trihedral are identified by the unit vectors $\hat{x}$, $\hat{y}$, and $\hat{z}$, as well as the origin. These are identified in Figure 4.

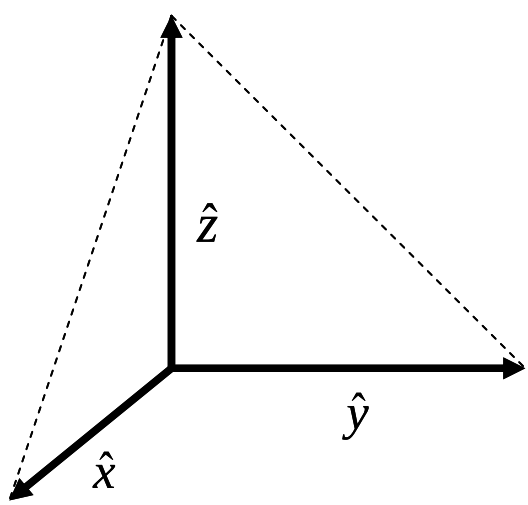

Figure 4. Vector definitions for relevant points that define the trihedral.

2.2 Treating Bounces using Images

What makes a trihedral corner reflector retro-reflective is a triple-bounce with one bounce each off of the two upright triangular plates, and one bounce off the bottom ground plate.

With some foresight, we will employ 'images' instead of dealing with the complex geometries involved with triple bounces.

In a single dimension, the image of the $\hat{z}$ vector across the x, y plane is the $-\hat{z}$ vector, illustrated in Figure 5.

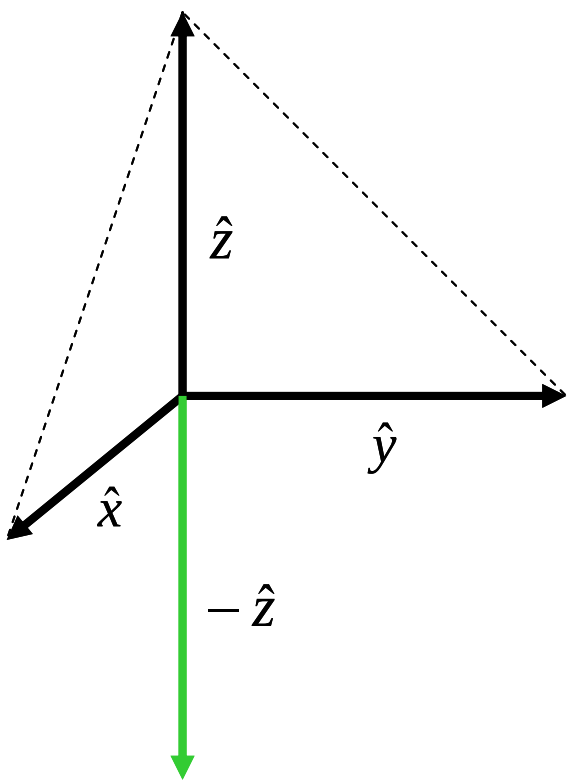

Figure 5. Image of vertical vector across x,y ground plane.

Since we have three orthogonal plates, the complete set of images for all unit vectors is illustrated in Figure 6. Herein we identify two squares. These are

1. a square identified with corners $\hat{x}$, $\hat{z}$, $-\hat{x}$, and $-\hat{z}$, and
2. a square identified with corners $\hat{y}$, $\hat{z}$, $-\hat{y}$, and $-\hat{z}$.

In addition, there is still the infinite ground plane that is the entire x, y plane.

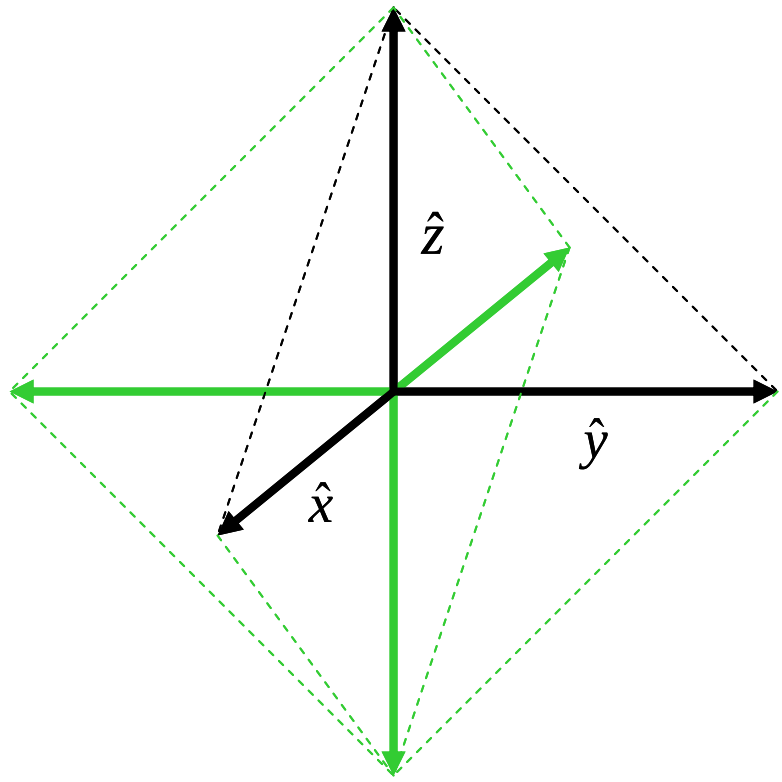

Figure 6. Image of defining vectors across all plates of trihedral, and the squares that they define.

Using the images, from a particular perspective, a triple bounce retro-reflection will occur over an effective area that is the intersection of the projections of the two squares in the direction of that particular perspective. An infinite ground plane does not further constrain the projected area. A limited extent ground plane would in fact constrain the projections even more at some perspectives, but an analytical solution for this case is outside the scope of this report.

The projections of either of the squares in any particular direction will generally be a parallelogram. The projection of the square will not necessarily be a square itself.

For example, for the perspective of Figure 6, the intersection of the two parallelograms is identified in Figure 7. For a different perspective, the intersection of the two parallelograms is given in Figure 8.

The intersection of the two parallelograms will itself be another parallelogram. The task at hand is to calculate the area of the intersection parallelogram, shaded in the figures, as a function of viewing perspective, that is elevation and azimuth angles. This is the effective area which is used for RCS calculation.

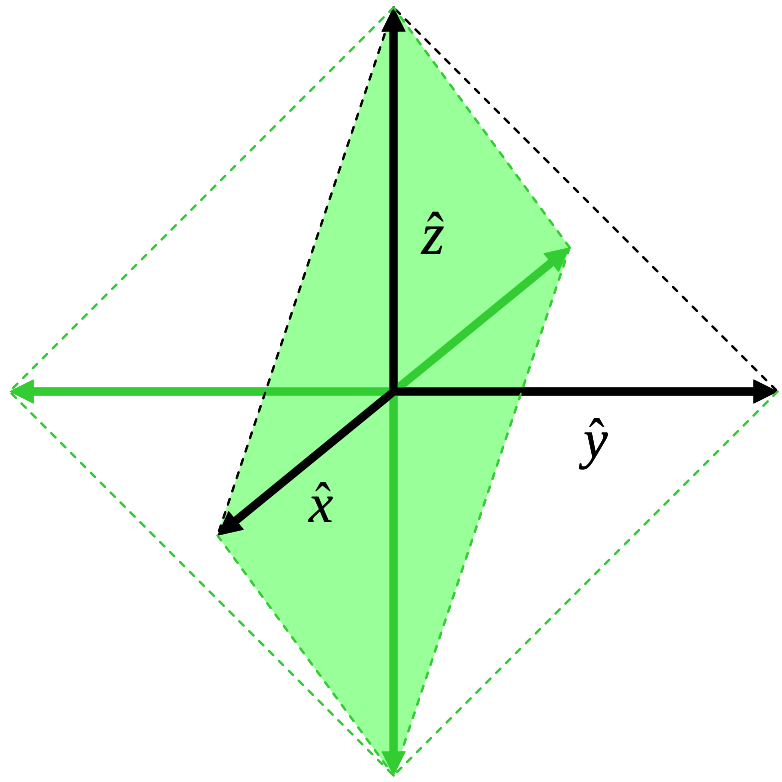

Figure 7. Intersection of projections of the two squares – Case 1.

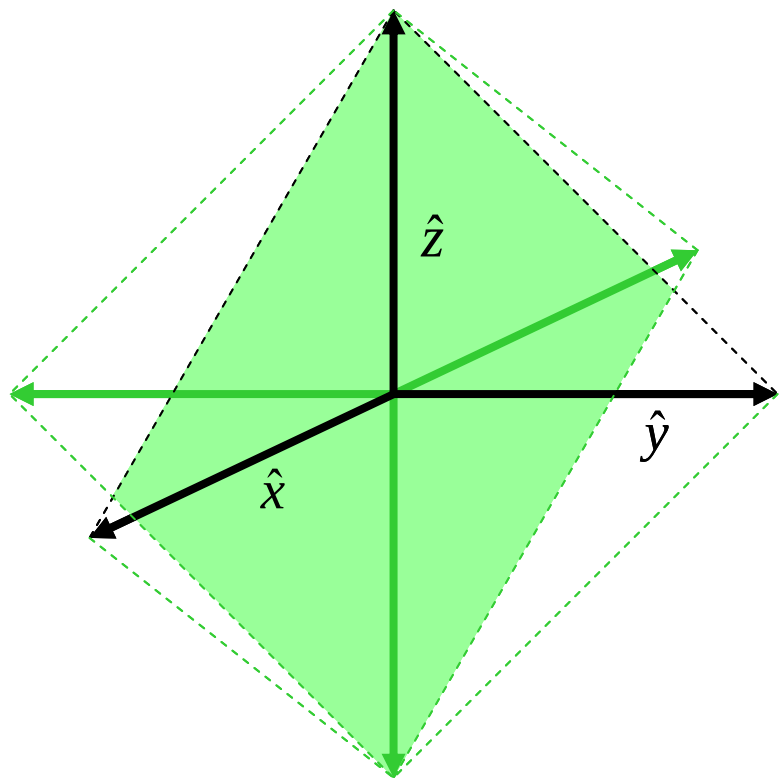

Figure 8. Intersection of projections of the two squares – Case 2.

2.3 Calculating Projected Area

The first step to calculating the projected area is to define the locations of the relevant points in the projection plane, that is in a plane that is normal to the projection direction defined by the azimuth and elevation angles.

We will use symmetry arguments to constrain our analysis to the space where $y \le 0$, as illustrated in Figure 9. In addition, we will concern ourselves for now with the azimuth angles $\theta \le \pi/4$.

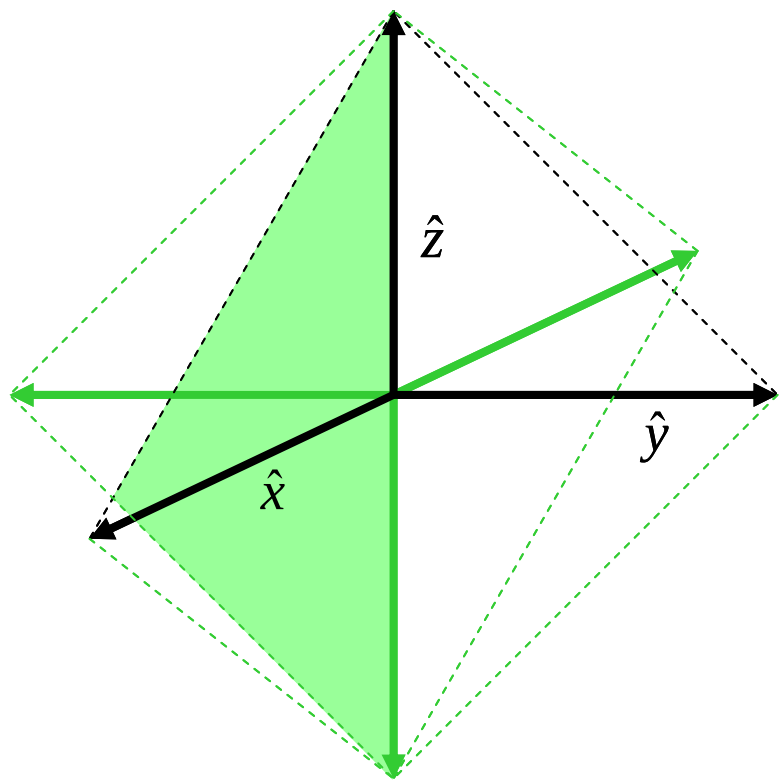

Figure 9. Triangular region that is one half the area of the intersection of the projection of the two squares. Case 2 is illustrated.

The problem is now reduced to finding the area of a triangle in both of two cases, depicted in Figure 10. The input to these calculations are the locations (coordinates) of the four identified points, Q_1 through Q_4. We also identify some useful interior angles.

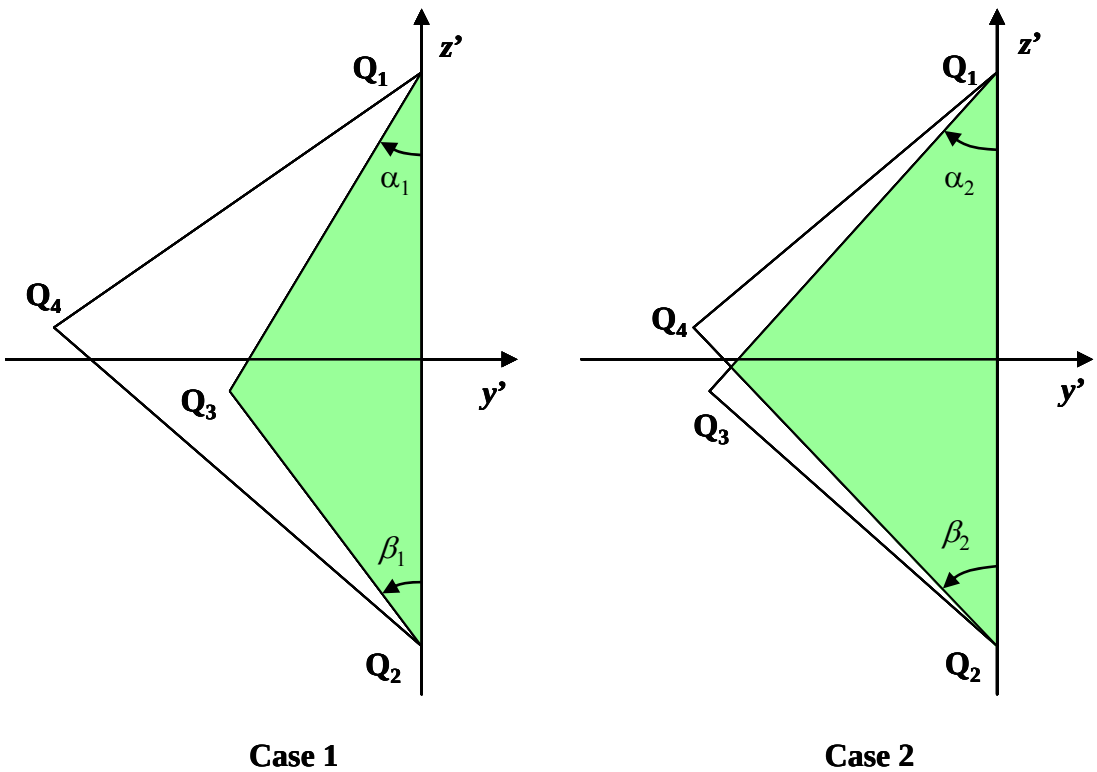

Figure 10. Triangular regions defined by the intersection of the projections of the two squares.

In the x, y, z coordinate frame, the four points correspond to the positions

$$
\begin{aligned}
Q_1 &: \quad \mathbf{p}_1 = [0 \quad 0 \quad 1]^T, \\
Q_2 &: \quad \mathbf{p}_2 = [0 \quad 0 \quad -1]^T, \\
Q_3 &: \quad \mathbf{p}_3 = [1 \quad 0 \quad 0]^T, \\
Q_4 &: \quad \mathbf{p}_4 = [0 \quad -1 \quad 0]^T, \quad (4)
\end{aligned}
$$

where the superscript 'T' denotes a transpose.

In the rotated x', y', z' coordinate frame, the four points correspond to the positions

$$
\begin{aligned}
Q_1 &: \quad \mathbf{p}'_1 = \mathbf{R}\,\mathbf{p}_1, \\
Q_2 &: \quad \mathbf{p}'_2 = \mathbf{R}\,\mathbf{p}_2, \\
Q_3 &: \quad \mathbf{p}'_3 = \mathbf{R}\,\mathbf{p}_3, \\
Q_4 &: \quad \mathbf{p}'_4 = \mathbf{R}\,\mathbf{p}_4, \quad (5)
\end{aligned}
$$

where the rotation matrix is given by

$$\mathbf{R} = \begin{bmatrix} \cos\theta\cos\psi & \sin\theta\cos\psi & \sin\psi \\ -\sin\theta & \cos\theta & 0 \\ -\cos\theta\sin\psi & -\sin\theta\sin\psi & \cos\psi \end{bmatrix}. \quad (6)$$

The result is expanded to

$$\begin{aligned}
Q_1: &\quad \mathbf{p}'_1 = \mathbf{R}\begin{bmatrix}0 & 0 & 1\end{bmatrix}^T = \begin{bmatrix}\sin\psi & 0 & \cos\psi\end{bmatrix}^T, \\
Q_2: &\quad \mathbf{p}'_2 = \mathbf{R}\begin{bmatrix}0 & 0 & -1\end{bmatrix}^T = \begin{bmatrix}-\sin\psi & 0 & -\cos\psi\end{bmatrix}^T, \\
Q_3: &\quad \mathbf{p}'_3 = \mathbf{R}\begin{bmatrix}1 & 0 & 0\end{bmatrix}^T = \begin{bmatrix}\cos\theta\cos\psi & -\sin\theta & -\cos\theta\sin\psi\end{bmatrix}^T, \\
Q_4: &\quad \mathbf{p}'_4 = \mathbf{R}\begin{bmatrix}0 & -1 & 0\end{bmatrix}^T = \begin{bmatrix}-\sin\theta\cos\psi & -\cos\theta & \sin\theta\sin\psi\end{bmatrix}^T. \quad (7)
\end{aligned}$$

In the y', z' plane, these are projected to the coordinates

$$\begin{aligned}
Q_1: &\quad \mathbf{q}'_1 = \begin{bmatrix}0 & \cos\psi\end{bmatrix}^T, \\
Q_2: &\quad \mathbf{q}'_2 = \begin{bmatrix}0 & -\cos\psi\end{bmatrix}^T, \\
Q_3: &\quad \mathbf{q}'_3 = \begin{bmatrix}-\sin\theta & -\cos\theta\sin\psi\end{bmatrix}^T, \\
Q_4: &\quad \mathbf{q}'_4 = \begin{bmatrix}-\cos\theta & \sin\theta\sin\psi\end{bmatrix}^T. \quad (8)
\end{aligned}$$

The interior angles of Figure 10 may be calculated as follows.

$$\begin{aligned}
\tan\alpha_1 &= \frac{\sin\theta}{\cos\psi + \cos\theta\sin\psi}, \\
\tan\beta_1 &= \frac{\sin\theta}{\cos\psi - \cos\theta\sin\psi}, \\
\tan\alpha_2 &= \tan\alpha_1 = \frac{\sin\theta}{\cos\psi + \cos\theta\sin\psi}, \\
\tan\beta_2 &= \frac{\cos\theta}{\cos\psi + \sin\theta\sin\psi}. \quad (9)
\end{aligned}$$

Based on these angles we can select whether we have case 1 or case 2 for a particular viewing perspective. Note that

$$\begin{aligned}
&\tan\beta_2 \geq \tan\beta_1 \quad \Rightarrow \text{ case 1, and} \\
&\tan\beta_2 < \tan\beta_1 \quad \Rightarrow \text{ case 2.}
\end{aligned} \quad (10)$$

This may be expanded, and then simplified to the rule

$$(\cos\theta - \sin\theta) \geq \tan\psi \quad \Rightarrow \text{ case 1, otherwise case 2.} \quad (11)$$

Case 1.

Using the results of Appendix B, the area of the triangle is

$$A_{tri} = \frac{(2\cos\psi)^2 \tan\alpha_1 \tan\beta_1}{2(\tan\alpha_1 + \tan\beta_1)} . \quad (12)$$

which is expanded to

$$A_{tri} = \frac{(2\cos\psi)^2 \left(\dfrac{\sin\theta}{\cos\psi + \cos\theta\sin\psi}\right)\dfrac{\sin\theta}{\cos\psi - \cos\theta\sin\psi}}{2\left(\dfrac{\sin\theta}{\cos\psi + \cos\theta\sin\psi} + \dfrac{\sin\theta}{\cos\psi - \cos\theta\sin\psi}\right)} . \quad (13)$$

This can be simplified to

$$A_{tri} = \sin\theta\cos\psi . \quad (14)$$

Case 2.

Using the results of Appendix B, the area of the triangle is

$$A_{tri} = \frac{(2\cos\psi)^2 \tan\alpha_2 \tan\beta_2}{2(\tan\alpha_2 + \tan\beta_2)} . \quad (15)$$

which is expanded to

$$A_{tri} = \frac{(2\cos\psi)^2 \left(\dfrac{\sin\theta}{\cos\psi + \cos\theta\sin\psi}\right)\dfrac{\cos\theta}{\cos\psi + \sin\theta\sin\psi}}{2\left(\dfrac{\sin\theta}{\cos\psi + \cos\theta\sin\psi} + \dfrac{\cos\theta}{\cos\psi + \sin\theta\sin\psi}\right)} . \quad (16)$$

This can be simplified to

$$A_{tri} = \frac{2\sin\theta\cos\theta\cos\psi}{(\sin\theta + \cos\theta + \tan\psi)} . \quad (17)$$

Combined Results for Area.

The two cases are combined to the following.

$$A_{tri} = \begin{cases} \sin\theta\cos\psi & \text{if } (\cos\theta - \sin\theta) \geq \tan\psi \\ \dfrac{2\sin\theta\cos\theta\cos\psi}{(\sin\theta + \cos\theta + \tan\psi)} & \text{else} \end{cases} \quad . \ (18)$$

We reiterate that this is just the area of the triangular region that represents one half the area of the intersection of the projections of the two squares defined by vectors and their images in the *x,z* and *y,z* planes.

The incorporation of this area into RCS calculations is performed in the next section.

2.4 Calculating RCS

Given the results of the previous section, we note that the total area of intersection of projections is twice A_{tri}. Furthermore, this assumes a unit edge for the trihedral edges that meet at the apex. A more general expression for RCS is then

$$\sigma(\psi,\theta) = \frac{4\pi}{\lambda^2}(2A_{tri})^2 a^4 \quad (19)$$

where

a = the edge of the triangular sections of the trihedral meeting at the apex. (20)

Consequently, for the trihedral on an infinite ground plate

$$\sigma(\psi,\theta) = \frac{16\pi\, a^4}{\lambda^2}(A_{tri})^2 \quad \text{where}$$

$$A_{tri} = \begin{cases} \sin\theta\cos\psi & \text{if } (\cos\theta - \sin\theta) \geq \tan\psi \\ \dfrac{2\sin\theta\cos\theta\cos\psi}{(\sin\theta + \cos\theta + \tan\psi)} & \text{else} \end{cases}, \quad (21)$$

but recall that that this assumed $\theta \leq \pi/4$. Due to symmetry arguments we expect the RCS at θ to be the same as at $\pi/2 - \theta$. This leads to the final equation for RCS as

$$\sigma(\psi,\theta) = \frac{16\pi\, a^4}{\lambda^2}(A_{tri})^2 \quad \text{where}$$

$$A_{tri} = \begin{cases} \sin\theta\cos\psi & \text{if } (\cos\theta - \sin\theta) \geq \tan\psi \\ \cos\theta\cos\psi & \text{if } (\sin\theta - \cos\theta) \geq \tan\psi \\ \dfrac{2\sin\theta\cos\theta\cos\psi}{(\sin\theta + \cos\theta + \tan\psi)} & \text{else} \end{cases}, \quad (22)$$

where this expression is good for $0 < \theta < \pi/2$, and $0 < \psi < \pi/2$.

“This is really something. I don't know what, but it's something.”

-- Crow T. Robot, Mystery Science Theater 3000 (MST3K)

3 Comparison to Conventional Triangular Trihedral Corner Reflector

In this section we compare the RCS of a triangular trihedral with infinite ground plate to the RCS of a more conventional triangular trihedral. To begin this discussion we borrow a section from an earlier report.[1] More conventional trihedrals are discussed in some detail in the literature, including by Ruck, et al.[2], Bonkowski, et al.[3], Crispen and Siegel[4], and Sarabandi and Chiu[5].

3.1 Review of Conventional Triangular Trihedral

Consider a trihedral with sides comprised of isosceles right triangles. With the geometry defined as in Figure 11, using geometrical optics, we identify the relative RCS as a function of orientation as

$$\sigma_{triangle}(\psi,\theta) = \begin{cases} \dfrac{4\pi}{\lambda^2} a^4 \left(\dfrac{4c_1c_2}{c_1+c_2+c_3} \right)^2 & \text{for} \quad c_1+c_2 \le c_3 \\ \dfrac{4\pi}{\lambda^2} a^4 \left(c_1+c_2+c_3 - \dfrac{2}{c_1+c_2+c_3} \right)^2 & \text{for} \quad c_1+c_2 \ge c_3 \end{cases} \quad (23)$$

where c_1, c_2, c_3 are each assigned one of

$$\left.\begin{matrix} c_1 \\ c_2 \\ c_3 \end{matrix}\right\} = \begin{cases} \sin\psi \\ \cos\psi \sin\theta \\ \cos\psi \cos\theta \end{cases} \quad (24)$$

such that $c_1 \le c_2 \le c_3$. The peak RCS of such a trihedral is calculating as

$$\sigma_{triangle,peak} = \frac{4\pi\, a^4}{3\lambda^2} \quad (25)$$

The direction of peak RCS, or the bore-sight of the trihedral, is in the direction $\theta = \pi/4$, or 45 degrees, and at a grazing angle of $\psi = \tan^{-1}\left(1/\sqrt{2}\right)$, or about 35.2644 degrees.

Figure 12 plots contours of constant RCS relative to peak value as a function of azimuth and elevation angles.

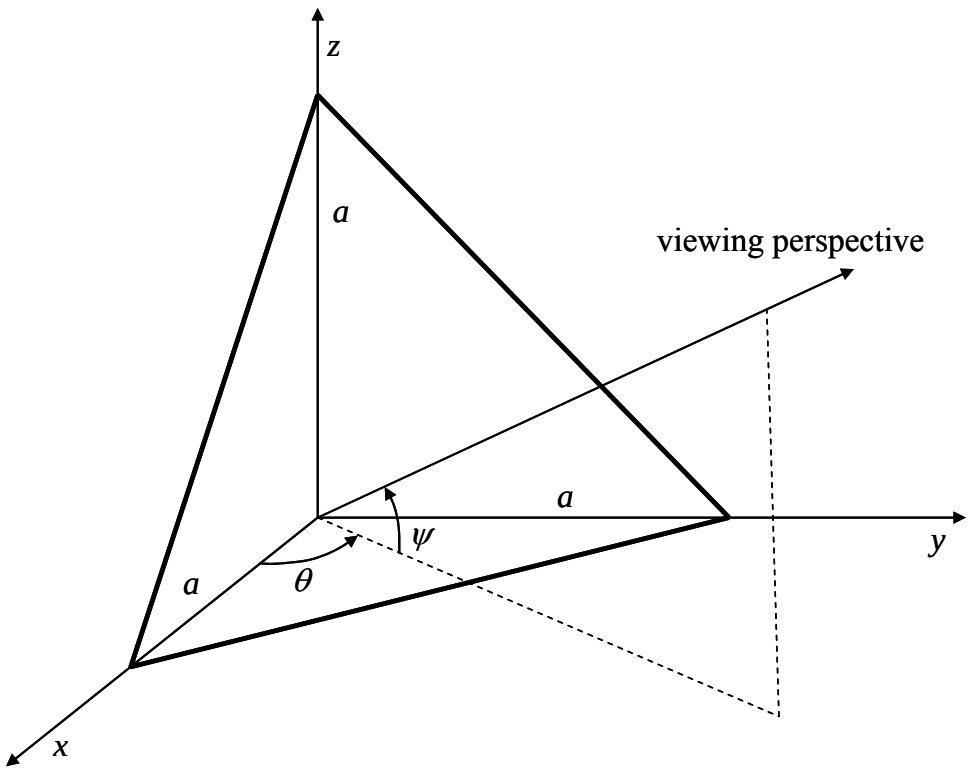

Figure 11. Geometry definition for RCS characteristics.

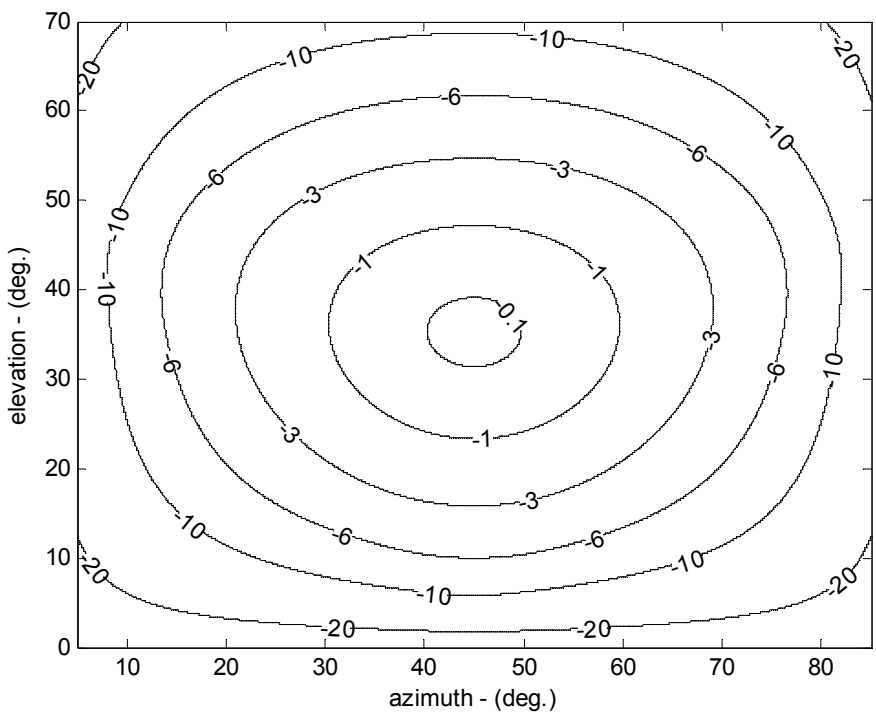

Figure 12. Contours of constant relative RCS for triangular trihedral corner reflector. Contour labels are in dBc.

3.2 Comparing Effects of Infinite Ground Plate

We wish now to compare the RCS of the trihedral with infinite ground plate to that of the conventional triangular trihedral. To make this meaningful, we wish to plot contours of a normalized RCS, that is, we will plot

$$\sigma_{normalized}(\psi,\theta) = \frac{\sigma(\psi,\theta)}{\sigma_{triangle,peak}} = 12(A_{tri})^2 \quad (26)$$

where

$$A_{tri} = \begin{cases} \sin\theta\cos\psi & if\ (\cos\theta - \sin\theta) \geq \tan\psi \\ \cos\theta\cos\psi & if\ (\sin\theta - \cos\theta) \geq \tan\psi \\ \dfrac{2\sin\theta\cos\theta\cos\psi}{(\sin\theta + \cos\theta + \tan\psi)} & else \end{cases} . \quad (27)$$

This normalized RCS is plotted in Figure 13. We note the following.

- In the bore-sight direction of the conventional trihedral, $\theta = 45$ degrees, and $\psi \approx 35.2644$ degrees, the infinite ground-plane trihedral exhibits a gain of about 2.5 dB.
- The direction of maximum RCS is at $\theta = 45$ degrees, and $\psi = 0$ degrees. That is, the RCS increases with shallower grazing angles.

Perhaps more interesting, we also identify a relative RCS of the trihedral with infinite ground plate compared to the conventional trihedral as a function of viewing perspective, that is

$$\sigma_{relative}(\psi,\theta) = \frac{\sigma(\psi,\theta)}{\sigma_{triangle}(\psi,\theta)} . \quad (28)$$

This is plotted in Figure 14. We note the following.

- The trihedral with infinite ground plate shows RCS substantially greater than that of the conventional trihedral, especially at shallow grazing angles. For example, at 4 degrees grazing angle, the improvement is better than 20 dB.
- The improvement is nearly constant for all azimuth angles.

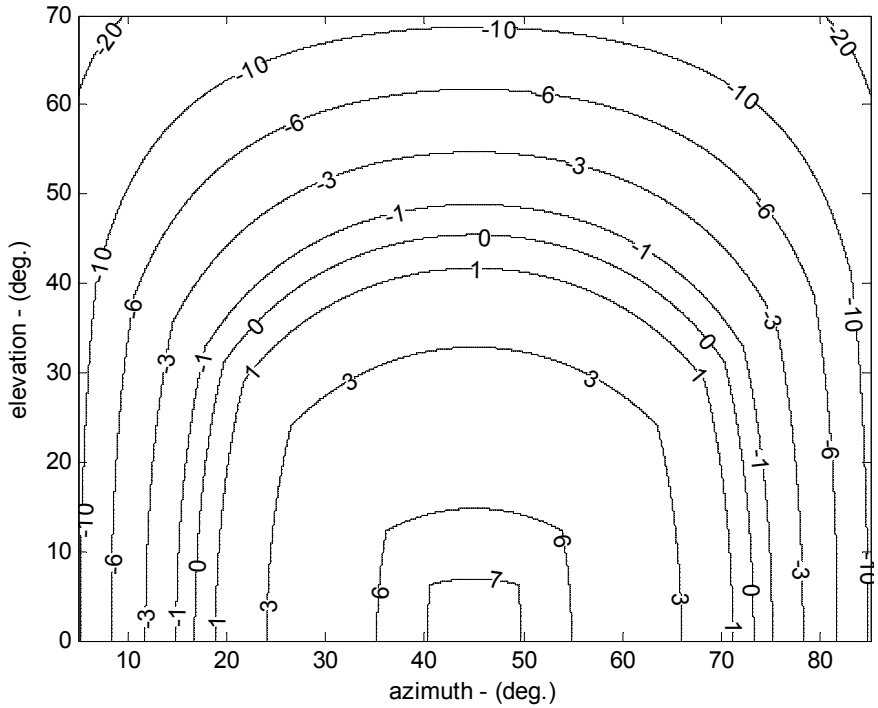

Figure 13. RCS of trihedral with infinite ground plane normalized to boresight RCS of conventional trihedral.

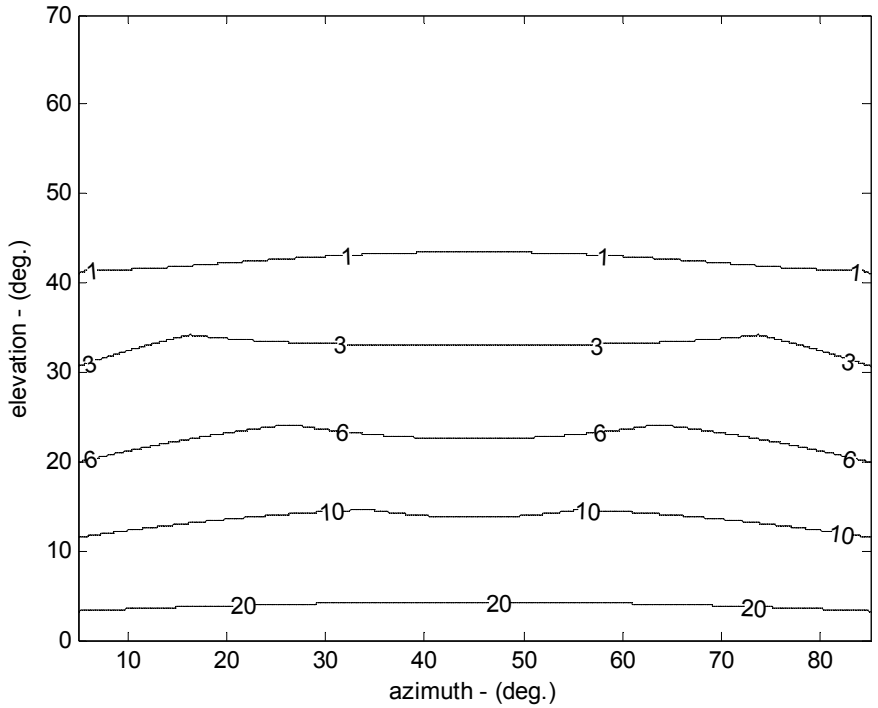

Figure 14. RCS of trihedral with infinite ground plane relative to RCS of conventional trihedral.

4 Some Practical Considerations

Of course, building a trihedral corner reflector with infinite ground plane poses a difficulty. More practical is a finite extent to the bottom plate, as might be exemplified in Figure 15. Using geometric optics, it becomes apparent that the RCS response of this arrangement will be equivalent to the infinite bottom plate over some limited extent of grazing angles, but will depart from that of the infinite plate at the shallower grazing angles. This is illustrated in Figure 16.

For a bottom plate with edge located a distance *b* from the trihedral apex, the infinite bottom plate RCS formula would be accurate as long as

$$\psi \geq \operatorname{atan}(a/b). \quad (29)$$

For example, if $b = 5a$, then the infinite ground-plane formula would be accurate for $\psi \geq 11.3$ degrees, and provide an RCS more than 11 dB brighter than the conventional trihedral with same dimension *a*.

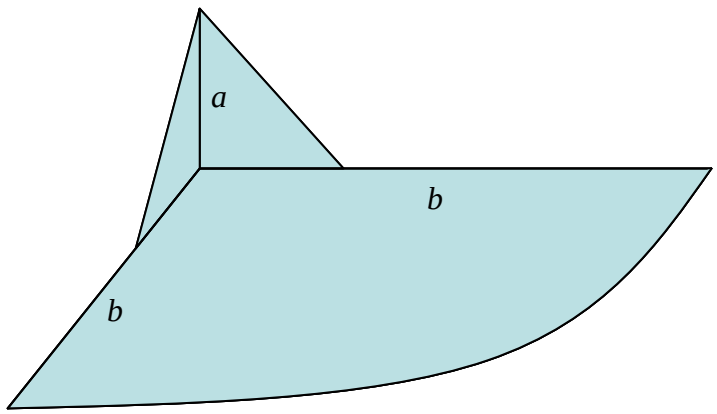

Figure 15. Trihedral on large but limited extent conducting plate.

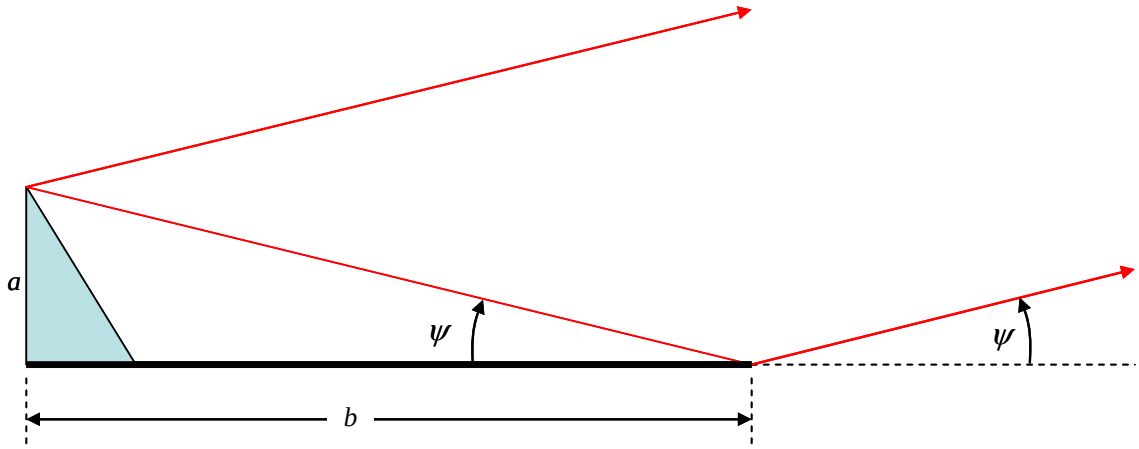

Figure 16. Illustration of grazing angle limit for the accuracy of the given RCS calculation.

Design Example

Consider a design requirement that calls for a +20 dBsm RCS at a 10 degree elevation angle using a physical geometry as illustrated in Figure 15. The wavelength is 18 mm, the center of Ku-band.

The task is to find dimensions *a* and *b*.

We begin by assuming $a = 1$. At a 45 degree azimuth angle and 10 degree elevation angle, the RCS is calculated to be 47.7 dB. Consequently we have an excess of 27.7 dB. This is corrected by adjusting the side-length to *a* = 20.23 cm.

At a 10 degree elevation angle, for there to be no ground bounce influencing the RCS, we need $b \geq 114.73$ cm.

We note that a conventional triangular trihedral would require *a* = 41.83 cm to achieve this in free space. However ground bounce in front of the trihedral would increase the RCS by an uncertain amount. The architecture of Figure 15 is superior in this regard.

5 Validation

The validity and usefulness of any new radar-cross-section formula based on geometric optics is open to question, so a demonstration of its validity is important. A comparison of the geometric RCS formula with other methods of computation can provide the validation needed. In this case, numerical computations for a specific example using the more rigorous methods will be compared with the prediction of the geometric formula. An extended trihedral with a corner-edge length of 150 mm and an extended bottom plate with radius 500 mm, illustrated in Figure 17, is used as a validation model. The computations are performed at 10 GHz, where the corner edge dimension is 5 wavelengths. The Shooting-and-Bouncing Ray (SBR) method and the Method of Moments (MoM) with the Multilevel Fast Multipole Algorithm (MLFMA) are the more rigorous methods used.

At 10 GHz, the Shooting-and-Bouncing Ray (SBR) method predicts the RCS of the standard trihedral in free space to be 4.4 dBsm at elevation 35.3° and azimuth 45°, and the RCS of the extend-plate trihedral with radius 500 mm to be 9.6 dBsm at elevation 15° and azimuth 45°. The predicted RCS of the extended-plate trihedral, using the new geometric formula is 9.7 dBsm at elevation 15° and azimuth 45°. The agreement is outstanding. The simple geometric RCS formula is a very good predictor of the RCS of a trihedral on a ground plane.

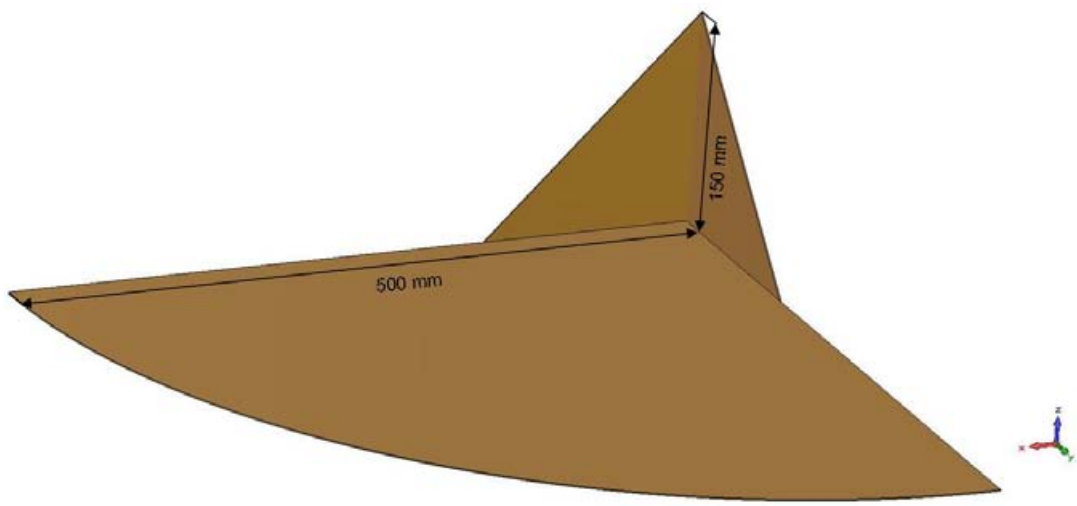

Figure 17. Extended trihedral with 150-mm corner edge and 500-mm extension radius.

For objects that are electrically large, measured in wavelengths, the physical optics method is useful for predicting scattering and radar cross section, unless currents that exist in the shadow region produce significant contributions to the scattered field. In the forward scattering region of a trihedral, there is essentially no contribution from currents in the shadow region, so physical optics methods are quite appropriate. The shooting and bouncing ray (SBR) method is an extension of physical optics, merging geometric optics with physical optics. The incident field is defined using geometric optics (tracing rays,

which are equivalent to plane-wave components), while the scattered field is computed with physical optics. It can be used efficiently to compute the scattered electromagnetic fields, radar cross-section, and, very importantly, the coupling and interaction between scattering surfaces for geometries that are very large with respect to a wavelength. As does physical optics, the SBR method computes the scattered field from an object by integrating surface currents (both electric and magnetic as appropriate) against the free-space Green's function to propagate the associated fields to the field point. It is generally more accurate than geometric optics, and provides a good comparison for appraising the reliability of the new geometric-optics model. It is especially well suited to computing the RCS of objects where multiple reflections are important, like the trihedral. The Xpatch® [6,7] implementation of the shooting and bouncing ray method is used to model the trihedral with the extended bottom plate. A good summary of Xpatch® capabilities is contained in the paper by Andersh.[8]

The extended-plate trihedral is also modeled with the SAIC Full-wave solver (SAF).[9] SAF is an electromagnetic-scattering computation program based on the Method of Moments (MoM) solution of the hybrid volume-surface integral equation. The SAF solver incorporates the Multilevel Fast Multipole Algorithm (MLFMA), and provides efficiency in computation speed and memory requirements. Since MoM incorporates the radiation condition into the formulation, no absorbing boundary is necessary. MoM and MLFMA codes are rigorous numerical solvers, and provide the highest level of computational accuracy, true to the physical laws of electromagnetism.

The MoM and SBR algorithms are similar in that they both are based on the equivalence principle. In fact, the only difference between MoM and SBR is the way in which the equivalent currents are computed. However, this is a *very* significant difference: MoM rigorously solves for the currents, while SBR approximates the currents using the physical-optics approximation. Once the currents are determined, though, both methods compute the scattered field by integrating the currents against the free-space Green's function.

The computed RCS for the trihedral with a corner edge of 150 mm is plotted as a function of both elevation and azimuth in Figure 18. The plot for the standard trihedral in free space is on the left, the extended-plate trihedral (with radius 500 mm) is in the middle (both computed with SBR), and the predicted RCS from the new geometric formula is on the right. When presented in this way, it is very clear that the extended-plate trihedral provides an enhanced RCS at low elevations, compared to the standard trihedral in free space. It is also clear that the new formula faithfully captures the important behavior.

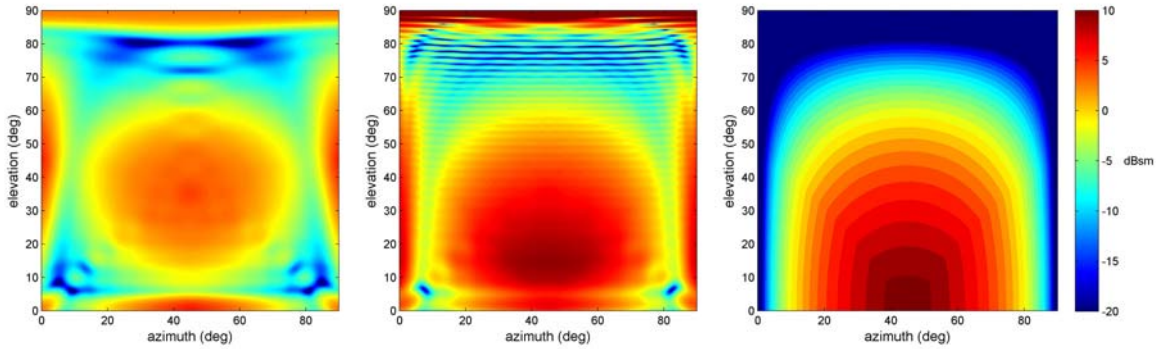

Figure 18. RCS at 10 GHz as a function of azimuth and elevation for the trihedral in free space on the left, the extended-plate trihedral in the middle (both computed with SBR), and the new geometric formula on the right.

Figure 19 shows the RCS computed from the new formula for the trihedral on an infinite ground plane (solid black curve) along with the RCS computed for the trihedral in free space and for the extended-plate trihedral with radii 500 mm and 1,000 mm. The corner edge of the trihedral is 150 mm in all cases. The predicted RCS is computed along an elevation arc located at azimuth 45°, in the vertical symmetry plane of the trihedral. The solid curves are computed with the SBR method, and the circles are computed with MLFMA. For elevations less than about 45°, the RCS of the extended-plate trihedral is greater than that of the equivalent standard trihedral in free space.

A similar comparison is displayed in Figure 20 as a function of azimuth, where the elevation is held constant at 15° for the extended-plate trihedral and 35.26° for the standard trihedral in free space. Of particular note is the approximately 4.5 dB stronger return for the extended-plate trihedral compared to the standard trihedral, especially noteworthy since the standard trihedral is observed at its optimum elevation. Its return is another 4 dB lower at an elevation of 15°, as can be seen in Figure 19.

As the comparisons in Figure 18 through Figure 20 demonstrate, the agreement between the predictions from the new geometric formula (black solid curve), the SBR predictions, and the MLFMA predictions is remarkable.

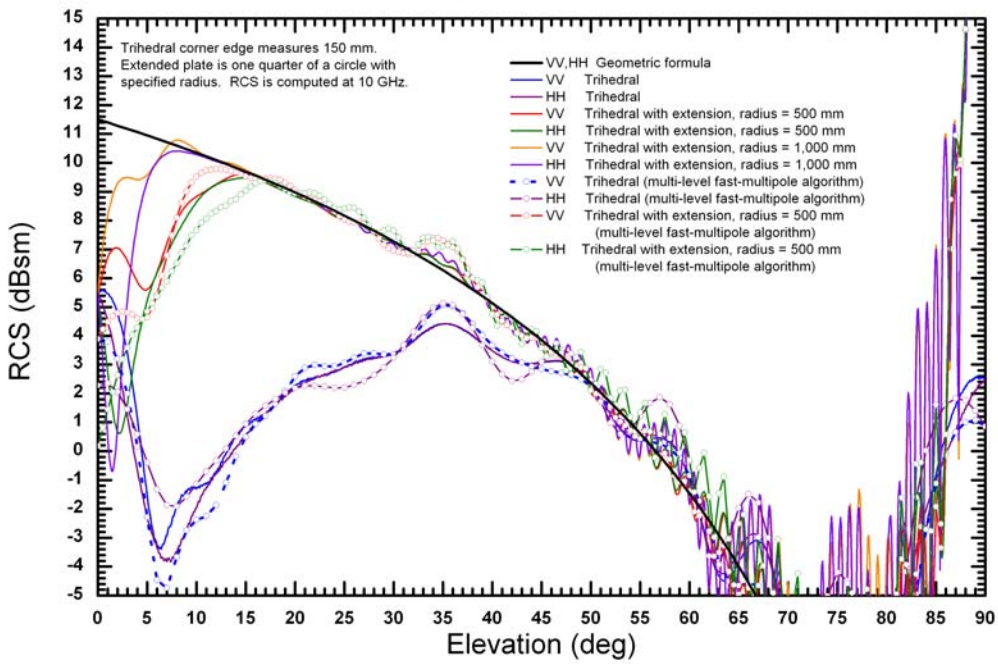

Figure 19. RCS at 10 GHz as a function of elevation at azimuth 45° for the extended-plate trihedral illustrated in Figure 1. RCS is computed with the SBR method for the solid curves and with the MLFMA method for the circles. The solid black curve is the model described in this report. The RCS of the equivalent standard trihedral in free space is also plotted.

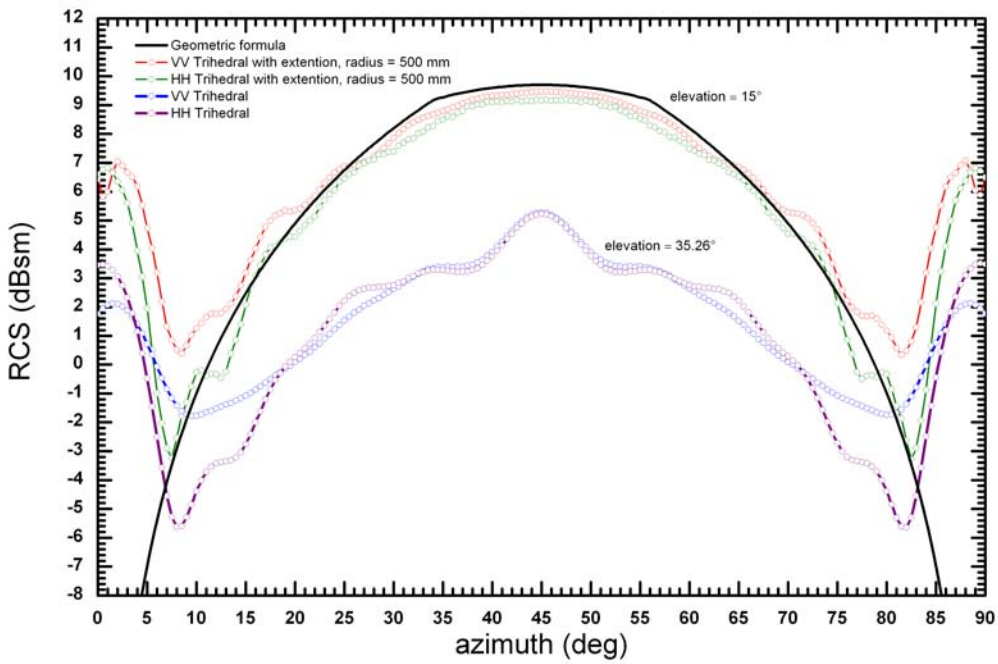

Figure 20. RCS at 10 GHz as a function of azimuth at elevation 15° for the extended-plate trihedral illustrated in Figure 17, and for the unmodified trihedral in free space at elevation 35.26°. RCS is computed with the multi-layer fast multipole integral equation method. The solid black curve is the model described in this report.

6 Conclusions

The following points are worth repeating.

- Conventional trihedral reflectors suffer degraded RCS at low grazing angles with respect to their bottom plate.
- A trihedral's RCS at low grazing angles can be enhanced by extending the lower conducting plate. Equations for RCS with an infinite bottom plate are presented.
- Even a limited extent to the bottom plate will improve low grazing angle performance. This will match the infinite plate equations out to some readily calculated grazing angle.
- The new geometric formula agrees remarkably well with more rigorous computations.

“Okay, what are we looking at and why are we looking at it?”

-- Tom Servo, Mystery Science Theater 3000 (MST3K)

Appendix A – Rotated Coordinate Frame

Consider the geometry of a rotated coordinate frame as in Figure 21.

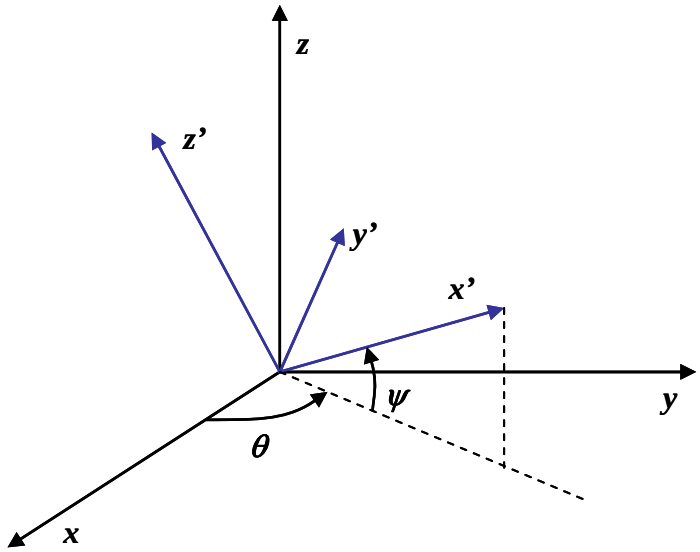

Figure 21. Angle definitions for rotated coordinate frame.

The question is "Given an arbitrary vector with coordinates in the x, y, z frame, what are its coordinates in the x', y', z' coordinate frame?"

Towards this end, we identify the new coordinate unit vectors as

$$\begin{aligned}
\hat{x}' &= \hat{x}\cos\theta\cos\psi + \hat{y}\sin\theta\cos\psi + \hat{z}\sin\psi\ , \\
\hat{y}' &= -\hat{x}\sin\theta + \hat{y}\cos\theta\ , \\
\hat{z}' &= \hat{x}\times\hat{y} = -\hat{x}\cos\theta\sin\psi - \hat{y}\sin\theta\sin\psi + \hat{z}\cos\psi\ . \quad \text{(A1)}
\end{aligned}$$

This can be described via a rotation matrix, where

$$\mathbf{R} = \begin{bmatrix} \cos\theta\cos\psi & \sin\theta\cos\psi & \sin\psi \\ -\sin\theta & \cos\theta & 0 \\ -\cos\theta\sin\psi & -\sin\theta\sin\psi & \cos\psi \end{bmatrix}. \quad \text{(A2)}$$

Consequently, some vector $\mathbf{p}$ with coordinates in the x, y, z frame, will have new coordinates in the x', y', z' coordinate frame described by

$$\mathbf{p}' = \mathbf{R}\,\mathbf{p}\ . \quad \text{(A3)}$$

Of note are the following.

- With this particular transformation, there is no 'twist' about the x' axis. While the rotation matrix developed herein is thereby somewhat less general, as it takes into account only two independent angles, this nevertheless serves the purpose of this report.

- The vector $\hat{z}$ is contained within the x', z' plane.

- Projections of an arbitrary vector $\mathbf{p}$ into a plane normal to x' will have coordinates in that plane of

  $\mathbf{q}' = (\mathbf{p} \bullet \hat{y}')\hat{y}' + (\mathbf{p} \bullet \hat{z}')\hat{z}'$. (A4)

<u>Decomposed Rotations</u>

We note that the final rotation matrix **R** can be decomposed into a rotation about the vertical axis *z* followed by a rotation about the axis *y'*. That is

$$\mathbf{R} = \mathbf{R}_{y'}\mathbf{R}_z \quad \text{(A5)}$$

where

$$\mathbf{R}_z = \begin{bmatrix} \cos\theta & \sin\theta & 0 \\ -\sin\theta & \cos\theta & 0 \\ 0 & 0 & 1 \end{bmatrix}, \text{(A6)}$$

and

$$\mathbf{R}_{y'} = \begin{bmatrix} \cos\psi & 0 & \sin\psi \\ 0 & 1 & 0 \\ -\sin\psi & 0 & \cos\psi \end{bmatrix}. \text{(A7)}$$

We confirm that

$$\mathbf{R} = \begin{bmatrix} \cos\theta\cos\psi & \sin\theta\cos\psi & \sin\psi \\ -\sin\theta & \cos\theta & 0 \\ -\cos\theta\sin\psi & -\sin\theta\sin\psi & \cos\psi \end{bmatrix} = \begin{bmatrix} \cos\psi & 0 & \sin\psi \\ 0 & 1 & 0 \\ -\sin\psi & 0 & \cos\psi \end{bmatrix} \begin{bmatrix} \cos\theta & \sin\theta & 0 \\ -\sin\theta & \cos\theta & 0 \\ 0 & 0 & 1 \end{bmatrix}. \quad \text{(A8)}$$

Appendix B – Area of Triangle from Angle-Side-Angle Information

The task at hand is to calculate the area of a triangle from initial knowledge of the length of one edge, and two angles. These quantities are illustrated in Figure 22.

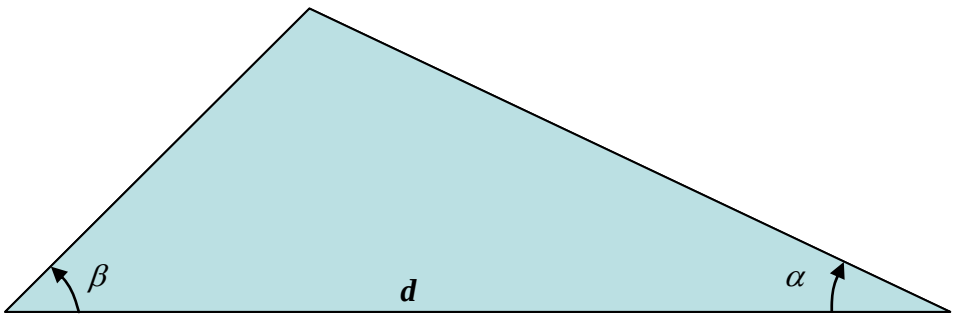

Figure 22. Trigonometric parameter definitions for triangle.

We approach this problem by dropping a perpendicular as illustrated in Figure 23.

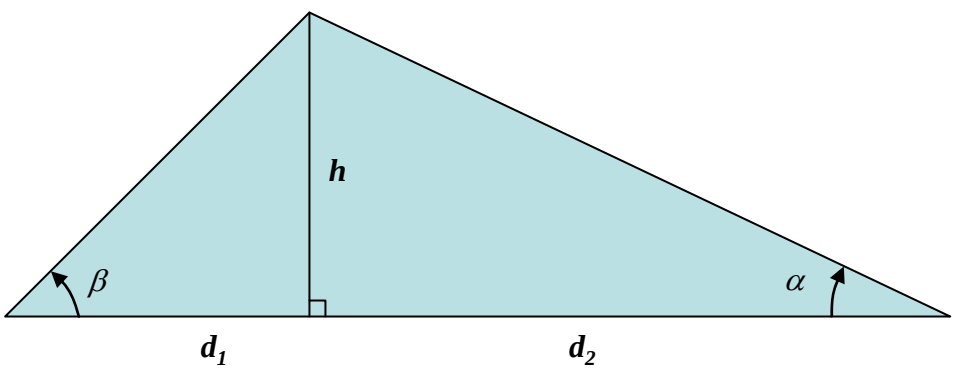

Figure 23. Additional trigonometric parameter definitions for triangle.

We observe that the height h is calculated as

$$h = d_1 \tan\beta = d_2 \tan\alpha \text{ . (B1)}$$

Furthermore, we identify that the total base length is

$$d = d_1 + d_2 \text{ . (B2)}$$

These observations may be combined to yield

$$(d - d_2)\tan\beta = d_2 \tan\alpha \text{ . (B3)}$$

This can be solved to yield

$$d_2 = \frac{d \tan\beta}{(\tan\alpha + \tan\beta)} \text{ . (B4)}$$

Combining with above, we can calculate

$$h = \frac{d \tan\alpha \tan\beta}{(\tan\alpha + \tan\beta)} \text{ . (B5)}$$

The area of the triangle is then calculated as

$$A_{tri} = \frac{d\,h}{2} = \frac{d^2 \tan\alpha \tan\beta}{2(\tan\alpha + \tan\beta)} \text{ . (B6)}$$

A little further manipulation shows that this is equivalent to a form that sometimes appears in the literature as

$$A_{tri} = \frac{d^2 \sin\alpha \sin\beta}{2\sin(\alpha + \beta)} \text{ . (B7)}$$

These are sometimes referred to as Angle-Side-Angle (ASA) formulas for the area of a triangle.

References

[1] Armin W. Doerry, "Reflectors for SAR Performance Testing", Sandia Report SAND2008-0396, Unlimited Release, January 2008.

[2] George T. Ruck, Donald E. Barrick, William D. Stuart, Clarence K. Krichbaum, *Radar Cross Section Handbook*, Vol. 2, SBN 306-30343-4, Plenum Press, 1970.

[3] R. R. Bonkowski, C. R. Lubitz, C. E. Schensted, "Studies in Radar Cross-Sections VI, Cross-Sections of Corner Reflectors and Other Multiple Scatterers at Microwave Frequencies", Project MIRO, UMM-106, University of Michigan Radiation Laboratory, October, 1953.

[4] J. W. Crispin, Jr., K. M. Siegel, *Methods of Radar Cross Section Analysis*, Academic Press, New York, 1968.

[5] K. Sarabandi, Tsen-Chieh Chiu, "Optimum corner reflectors for calibration of imaging radars", *IEEE Transactions on Antennas and Propagation*, Volume: 44, Issue: 10, pp. 1348-1361, Oct 1996.

[6] *Xpatch Advanced EM Topics*, Xpatch® code suite, ver. 4.7, SAIC / DEMACO, a division of Science Applications International Corporation.

[7] *Xpatch*® code suite, ver. 4.7, SAIC / DEMACO, a division of Science Applications International Corporation.

[8] D. Andersh, *et al*, "XPATCH 4: The Next Generation in High Frequency Electromagnetic Modeling and Simulation Software", *The Record of the IEEE 2000 International Radar Conference*, 7-12 May 2000, pp 844-849.

[9] C. Lu and S. W. Lee, *Documents of Computer Code SAF: Volume 1, User Manual of SAF*, *Version 3.1*, SAIC/DEMACO, Champaign, October, 2005.

Distribution

Unlimited Release

1	MS 1330	B. L. Burns	5340	
1	MS 0519	T. J. Mirabal	5341	
1	MS 1330	M. S. Murray	5342	
1	MS 1330	W. H. Hensley	5342	
1	MS 1330	S. D. Bensonhaver	5342	
1	MS 1330	T. P. Bielek	5342	
1	MS 1330	J. D. Bradley	5342	
1	MS 1330	A. W. Doerry	5342	
1	MS 1330	D. W. Harmony	5342	
1	MS 1330	J. A. Hollowell	5342	
1	MS 1330	C. Musgrove	5342	
1	MS 1330	S. Nance	5342	
1	MS 1332	R. Riley	5342	
1	MS 1330	J. A. Rohwer	5342	
1	MS 1330	B. G. Rush	5342	
1	MS 1330	G. J. Sander	5342	
1	MS 1330	D. G. Thompson	5342	
1	MS 0501	P. R. Klarer	5343	
1	MS 1330	K. W. Sorensen	5345	
1	MS 0529	B. C. Brock	5345	
1	MS 1330	D. F. Dubbert	5345	
1	MS 0529	G. K. Froehlich	5345	
1	MS 1330	F. E. Heard	5345	
1	MS 1330	G. R. Sloan	5345	
1	MS 1330	S. M. Becker	5348	
1	MS 1330	O. M. Jeromin	5348	
1	MS 1330	S. A. Hutchinson	5349	
1	MS 0519	D. L. Bickel	5354	
1	MS 0519	A. Martinez	5354	
1	MS 0899	Technical Library	9536	(electronic copy)

;-)